information services
gwasanaethau gwybodaeth

Reversed T cell receptor docking on a Major Histocompatibility Class I complex within the naïve T cell repertoire limits involvement in the immune response

Stephanie Gras[1,2*,] Jesseka Chadderton[1,3*], Claudia M. Del Campo[1,2], Carine Farenc[1], Florian Wiede[1], Tracy M. Josephs[1,2], Xavier Y.X. Sng[1,3] Michiko Mirams[3], Katherine A. Watson[3], Tony Tiganis[1], Kylie M. Quinn[1,3], Jamie Rossjohn[1,2,4#] & Nicole L. La Gruta[1,3#]

[1]Infection and Immunity Program and Department of Biochemistry and Molecular Biology, Biomedicine Discovery Institute, Monash University, Clayton, Victoria 3800, Australia

[2]ARC Centre of Excellence in Advanced Molecular Imaging, Monash University, Clayton, Victoria 3800, Australia

[3]Department of Microbiology and Immunology, Peter Doherty Institute for Infection and Immunity, University of Melbourne, Parkville, Victoria 3010, Australia

[4]Institute of Infection and Immunity, Cardiff University School of Medicine, Heath Park, Cardiff CF14 4XN, UK

[*] joint first authors

[#] joint senior and corresponding authors. E-mail: Jamie.rossjohn@monash.edu, nicole.la.gruta@monash.edu

Running title: Reversed TCR docking in the naïve CD8^{+} T cell repertoire

Abstract

The anti-viral T cell response is drawn from the naïve T cell repertoire. During influenza infection, the CD8$^+$ T cell response to an H-2D^b-restricted nucleoprotein epitope (NP$_{366}$) is characterized by preferential expansion of TRBV13-1$^+$ T cells and avoidance of TRBV17$^+$ T cells, despite the latter dominating the naïve precursor repertoire. Two TRBV17$^+$ TCRs bound H-2D^b-NP$_{366}$ with a 180° reversed polarity compared to the canonical TCR-pMHC-I docking. The TRBV17 β-chain dominated the interaction and, while the CDR3 loops exclusively mediated contacts with the MHC-I, peptide specificity was attributable to germline-encoded recognition. Nevertheless, the TRBV17$^+$ TCR exhibited moderate affinity towards H-2D^b-NP$_{366}$ and signaled effectively. Thus, the naïve CD8$^+$ T cell pool can comprise TCRs adopting reversed pMHC-I docking modes that limit their involvement in the immune response.

Introduction

The immune system can theoretically produce 10^{15}-10^{20} different αβT cell receptors (TCRs) (Davis and Bjorkman, 1988). Limitations imposed by thymic selection events causes the number of T cells in the naïve TCR repertoire to be reduced to ~2 x 10^6 in mice and around 2.5 x 10^7 in humans. Although substantial diversity remains in the naïve T cell repertoire, antigen-driven immune responses tend to exhibit highly reproducible TCR characteristics, or TCR bias, the extent of which can vary (Turner et al., 2006). In many cases, such antigen-driven biases are observed across multiple individuals suggesting reproducible selection of those characteristics.

While some TCR bias may be 'encoded' in the naïve epitope-specific T cell repertoire, studies in TCR transgenic systems (Malherbe et al., 2004; Zehn et al., 2009) and endogenous polyclonal T cell populations (Busch and Pamer, 1999; Cukalac et al., 2015; La Gruta et al., 2010; Neller et al., 2015; Price et al., 2005) reveal that antigen-driven biases often arise during the immune response, as a consequence of selective recruitment and/or prolonged expansion of particular T cells. Indeed, the ability to directly compare endogenous, polyclonal epitope-specific CD8$^+$ T cell repertoires before (Moon et al., 2007; Obar et al., 2008) and after antigen-driven expansion, has shown that archetypal TCR biases that define antigen-specific CD8$^+$ T cell repertoires in humans and mice are not necessarily reflected in the naïve T cell pool (Cukalac et al., 2015; La Gruta et al., 2010; Neller et al., 2015).

Although it is generally accepted that recruitment from the available epitope-specific T cell pool is comprehensive (van Heijst et al., 2009; Zehn et al., 2009), several studies have shown incomplete recruitment of T cell precursors. For example, analysis of epitope-specific TCRβ transgenic CD4$^+$ and CD8$^+$ T cells identified clones in the naïve repertoires that were not utilized in the immune response (Coles et al., 2003; Malherbe et al., 2004). Incomplete CTL precursor recruitment was also observed for endogenous CD8$^+$ T cell populations following either vesicular stomatitis virus (VSV) or influenza A virus (IAV) infection of mice (La Gruta et al., 2010; Obar et al., 2008), and depletion of Treg cells prior to infection with *Listeria monocytogenes* resulted in the elicitation of a novel CD8$^+$ T cell population (Pace et al., 2012).

In addition to selection occurring at the level of T cell recruitment, once recruited, T cell clones show differing profiles of expansion. For example, while a broad range of precursors may undergo initial rounds of division, prolonged expansion is observed for those clones that recognize cognate pMHC

with relatively high affinity (Busch and Pamer, 1999; Malherbe et al., 2004; Price et al., 2005; Zehn et al., 2009). Consequently, the immune population becomes dominated by clones expressing optimal TCR characteristics (Miles et al., 2011; Turner et al., 2006). This is observed following HIV infection, where particular TCRs selected after natural infection have been associated with superior virus control (Chen et al., 2012; Dong et al., 2004), and in the HLA-A2-restricted CTL response to the IAV matrix-derived peptide $M1_{58-66}$, where the response is comprised almost exclusively of $TRBV19^+$ T cells, despite diverse TRBV usage in the naïve repertoire (Neller et al., 2015). Collectively, these data reflect varying profiles of recruitment and expansion from the naïve T cell population that can significantly alter the profile of TCR usage in the immune response.

During primary IAV infection of B6 mice, the immunodominant $CD8^+$ T cell response is directed to an $H-2D^b$-restricted nucleoprotein epitope (NP_{366}) (Townsend et al., 1986), and is characterized by the preferential expansion of $TRBV13-1^+$ T cells from the naïve repertoire (Deckhut et al., 1993; La Gruta et al., 2010). In contrast, the $TRBV17^+$ T cell population, despite comprising around 25% of all naïve $H-2D^b$-NP_{366}-specific cells, contributes minimally to the immune response following viral infection (Cukalac et al., 2015). The $TRBV17^+$ $H-2D^b$-NP_{366}-specific T cells thus provide a unique opportunity to interrogate the characteristics of a TCR-pMHC-I interaction that lacks the capacity for efficient immune selection. To date, our structural understanding of TCR recognition of pMHC-I is based largely on TCRs identified from immune repertoires (Rossjohn et al., 2015).

We determined the structure of two $TRBV17^+$ TCRs from the naïve $CD8^+$ T cell repertoire in complex with $H-2D^b$-NP_{366}, and revealed a reversed docking topology relative to the established TCR-pMHC-I docking paradigm (Rossjohn et al., 2015), yet analogous to the reversed docking recently seen in the MHC-II system from a TCR isolated from an induced Treg cell (Beringer et al., 2015). Thus, naturally occurring T cells in the naïve pool express TCRs with reversed polarity pMHC-I docking modes that confer antigen specificity and functionality, but limit their ability to contribute to the immune response.

4

Results

Poor expansion of TRBV17$^+$ H-2D^b-NP$_{366}$-specific CD8$^+$ T cells

Comparison of TCR usage in CD8$^+$ T cell populations specific for the IAV-derived NP$_{366}$ epitope presented by H-2D^b, before and after infection, revealed a dominance (~25%) of TRBV17 usage in the naïve repertoire, that falls to below 1% (1/149 sequences) following IAV infection (Cukalac et al., 2015). The loss of TRBV17 representation is partly compensated by increased TRBV13-1 TCR usage from naïve (18%) to immune (~30-60%) T cell repertoires. To confirm the relative prevalence of TRBV17 and TRBV13-1 usage in immune H-2D^b-NP$_{366}$-specific populations, H-2D^b-NP$_{366}$ tetramer$^+$ CD8$^+$ populations, isolated from lung draining lymph node (mediastinal lymph node; mLN), spleen, and bronchoalveolar lavage (BAL) isolated at the peak of the CD8$^+$ T cell response (d10 after infection), were stained with antibodies specific for TRBV17 (anti-Vβ9) and TRBV13-1 (anti-Vβ8.3). Confirming our earlier results derived from TCR sequence analysis (Cukalac et al., 2015), TRBV13-1$^+$ T cells comprised around 50% of H-2D^b-NP$_{366}$-specific cells across all tissues, while <1% of T cells were TRBV17$^+$ (**Fig. 1a,b**). Similar results obtained at d7 after IAV infection demonstrated that, despite their prevalence in the naïve T cell repertoire, TRBV17$^+$ T cells contributed minimally over the course of the antiviral CTL response (**Fig. 1b**). Importantly, like TRBV13-1$^+$ H-2D^b-NP$_{366}$-specific T cells, the TRBV17$^+$ subset showed upregulated CD44 expression after infection, indicative of activation and recruitment into the response (**Fig. 1a**). Combined with our previous observation that the naïve H-2D^b-NP$_{366}$-specific CTL precursor pool is comprehensively recruited into the response (La Gruta et al., 2010), these data suggest that the paucity of TRBV17$^+$ H-2D^b-NP$_{366}$-specific T cells in the immune response is due to a failure to undergo extensive proliferation once recruited. Accordingly, TRBV17$^+$ H-2D^b-NP$_{366}$-specific T cells, whilst highly abundant in the naïve CD8$^+$ T cell repertoire, are very rare in the immune repertoire.

TRBV17$^+$ H-2D^b-NP$_{366}$-specific T cells show moderate affinity for pMHC-I

Following antigen encounter, comprehensive CD8$^+$ T cell recruitment, but truncated expansion, is a characteristic of CD8$^+$ T cells with relatively low pMHC-I affinity (Zehn et al., 2009). To determine the relative TCR avidity of TRBV17$^+$ and TRBV13-1$^+$ cells, the MFI of H-2D^b-NP$_{366}$ tetramer staining on d10 immune populations was determined. Tetramer MFI was significantly lower on polyclonal TRBV17$^+$ T cells compared to TRBV13-1$^+$ T cells at d10 post-infection (**Fig. 1c**), despite an overall similar level of TCR expression (**Supplemental Fig. 1a**), indicative of a lower avidity of TRBV17$^+$ TCRs for H-2D^b-NP$_{366}$, relative to the TRBV13-1$^+$ T cell subset.

We next transfected 293T cells with five TRBV13-1[+] TCRs and two TRBV17^{+} TCRs (NP1-B17 and NP3-B17), (**Supplemental Table 1**) identified from the H-2D^b-NP$_{366}$-specific repertoire (Cukalac et al., 2014; Cukalac et al., 2015). For a given amount of surface TCR expression (**Fig. 1d** and data not shown), all five TRBV13-1[+] TCRs bound significantly more tetramer than the TRBV17^{+} TCRs, which could only detectably bind tetramer at high TCR levels (**Fig. 1d,e**), again indicating a reduced TRBV17^{+} TCR affinity for H-2D^b-NP$_{366}$ compared to TRBV13-1[+] TCRs. Next, to determine the affinity of the TRBV17^{+} TCR for H-2D^b-NP$_{366}$, we expressed two soluble TRBV17^{+} TCRs (NP1-B17 and NP2-B17) (**Supplemental Table 1**) (Cukalac et al., 2015) and performed surface plasmon resonance (SPR) analysis (**Table 1** and **Fig. 1f**). The TRBV17^{+} TCRs bound H-2D^b-NP$_{366}$ with a dissociation constant (K$_d$) of ~40 and 30 μM, for NP1-B17 and NP2-B17, respectively, which is well within the established range of TCR-pMHC-I binding affinities (K$_d$ = ~1-100 μM), but at the lower end of the spectrum for viral epitope recognition (typically 1-10 μM) (Rossjohn et al., 2015). Accordingly, the TRBV17^{+} TCRs have a lower avidity than TRBV13-1[+] TCRs.

Inefficient H-2D^b-NP$_{366}$-specific TRBV17^{+} T cell expansion is intrinsic

To further assess the relative potential of TRBV17^{+} and TRBV13-1[+] H-2D^b-NP$_{366}$-specific T cells after antigen encounter, TCR retrogenic (Rg) mice were generated (Holst et al., 2006), expressing either a TRBV17^{+} (NP1-B17) TCR or a TRBV13-1^{+} TCR (NP1-B13) (**Supplemental Table 1**). Post-reconstitution, both TRBV17^{+} and TRBV13-1^{+} naïve Rg CD8^{+} T cells bound H-2D^b-NP$_{366}$ tetramer (**Fig. 1g**), although, notably, the TRBV17^{+} T cells bound tetramer more poorly than the TRBV13^{+} T cells. Adoptive transfer to recipient wildtype (WT) mice of equivalent numbers of TRBV17^{+} and TRBV13-1^{+} Rg CD8^{+} T cells either in combination or alone, followed by IAV infection (**Fig. 2a**), resulted in a notably larger number of TRBV13-1^{+} (compared to TRBV17^{+}) cells by d10 (**Fig. 2b**). This was observed across multiple tissues, and represented an average expansion of 1400-fold for TRBV13-1^{+} T cells and 150-fold for TRBV17^{+} T cells (**Fig. 2b**).

Polyfunctionality in T cells has been correlated with improved disease outcomes (Seder et al., 2008). Functional analysis of the TRBV17^{+} and TRBV13-1^{+} Rg CD8^{+} T cells after IAV infection revealed distinct cytokine profiles associated with the extent of division. Namely, a significantly larger percentage of TRBV13-1[+], compared to TRBV17^{+}, Rg cells from both lung and spleen produced IFNγ after short term *in vitro* peptide-specific restimulation, irrespective of whether the Rg cells were

transferred independently or together (**Fig. 2c** and **Supplemental Fig. 1b**). Of those IFNγ$^+$ cells, a significantly larger proportion of the TRBV13-1$^+$ T cells, compared to TRBV17$^+$ T cells, also produced TNF, although no difference was observed in the percentage of IFNγ$^+$ cells producing IL-2 (**Fig. 2c**), nor in the percentage or MFI of granzyme B producing cells (**Supplemental Fig. 1c,d**).

Given these observations, we assessed the relative abilities of the TRBV17$^+$ and TRBV13-1$^+$ T cells to transduce a signal upon TCR ligation. Here, ERK1/2 T202/Y204 phosphorylation was detected in Rg T cells. In the absence of peptide, no signal was detected from either the TRBV13-1$^+$ or the TRBV17$^+$ Rg cells, showing that recognition of pMHC-I was epitope-specific, whereas robust ERK1/2 T202/Y204 phosphorylation was evident after crosslinking either TCR with anti-CD3ε Ab (**Fig. 2d**). In the presence of the NP$_{366}$ peptide, phosphorylated ERK1/2 could be detected in both TRBV13-1$^+$ and TRBV17$^+$ Rg cells at 10 minutes post-activation, but at 45 min only the TRBV13-1$^+$ cells were able to maintain detectable levels of phosphorylated ERK1/2 (**Fig. 2d**).

Collectively, while TRBV17$^+$ T cells are recruited into the H-2D^b-NP$_{366}$-specific response, they are intrinsically inferior to the TRBV13-1$^+$ subset with respect to both proliferative capacity and functionality, which is associated with a reduced signaling capacity and moderate affinity for pMHC-I.

Reversed polarity of TRBV17$^+$ TCR recognition of H-2D^b-NP$_{366}$

To investigate the structural basis for the poor TRBV17+ T cell recruitment, we refolded two TRBV17$^+$ TCRs (NP1-B17 and NP2-B17, **Supplemental Table 1**), and determined the structure of the ternary complexes (**Fig 3**, **Supplemental Table 2**). These two TCRs differ in their CDR3α and CDR3β sequences (**Supplemental Table 1**), thereby also providing insight into how this variability impacted on H-2D^b-NP$_{366}$ recognition. The two TRBV17$^+$ TCRs docked onto the H-2D^b-NP$_{366}$ complex in a very similar fashion (**Fig. 3a,b**) but, strikingly, with a reversed topology compared to all other TCR-pMHC-I structures solved to date (**Fig. 3c**) (Rossjohn et al., 2015). Namely, whilst the α- chain and β-chain of previously published TCRs were universally observed to dock over the α2- and α1-helix of MHC-I, respectively (**Fig. 3c**), the α- and β-chains of the TRBV17$^+$ TCRs sat over the α1- and α2-helices, respectively (**Fig. 3a,b**). Here, the TRBV17$^+$ TCRs were located at the carboxy-terminal end of the H-2D^b antigen-binding cleft, forming a docking angle of 237° (**Fig. 3a,b**), which is approximately 180° from the mean docking angle (~63°) typically observed for TCR-pMHC-I interactions (**Fig. 3c**) (Rossjohn et al., 2015). The reversed docking observed for the TRBV17$^+$ TCRs were distinct from that

of the iTreg TCR-pHLA-DR4 complexes recently described (Beringer et al., 2015) (**Fig. 3d** and **Supplemental Fig. 2a**). Indeed, the TRBV17^{+} TCRs-H-2D^b-NP$_{366}$ docking footprints were more reminiscent of the KIR3DL1-pHLA-I interaction (Vivian et al., 2011) (**Supplemental Fig. 2b**).

As the NP1-B17 and NP2-B17 TCRs docked similarly onto the H-2D^b-NP$_{366}$ complex (**Fig. 3a,b**) (root mean square deviation of 0.81 Å on the overall complex), we describe below the molecular basis of the higher resolution complex, namely the NP1-B17 TCR. Despite the reversed polarity of TCR docking, the NP1-B17 TCR-H-2D^b-NP$_{366}$ binding was typical with respect to both buried surface area (BSA) at the TCR-pMHC-I interface (~1,870 Å^2 compared to an average of ~1,900 Å^2) (Rossjohn et al., 2015) and the extent of interactions with the MHC-I molecule (**Table 2**). Here, the TCR α-chain played a limited role (30% BSA) in interacting with H-2D^b-NP$_{366}$. Specifically, only the CDR3α loop contacted H-2D^b-NP$_{366,}$ while the germline-encoded regions of the TCR α-chain were too remote from the interface to contribute to binding (**Fig. 3a**). In contrast, the TCR β-chain contributed 70% of the BSA, underscoring the TRBV17 bias towards H-2D^b-NP$_{366}$ (see below). Here, the CDR2β loop (26% BSA) and the framework region of the β chain (FWβ) region (37% BSA) contributed substantially to the interaction with the H-2D^b-NP$_{366}$ (**Fig. 3a**). Accordingly, MHC-I restricted TCRs, isolated from the naïve T cell repertoire, can adopt a reversed TCR-pMHC-I docking topology.

Atypical contacts underpin the TRVB17^{+} TCR-H-2D^b interaction

The NP1-B17 and NP2-B17 TCRs bound two regions of MHC-I that have not been previously observed to mediate TCR binding (**Table 2, Fig. 3ab** and **Fig. 4a**). Namely, the CDR3α loop bound two H-2D^b loops (residues 14-21 and 85-92) that are situated outside of the antigen-binding cleft, being located after the first β-strand and at the end of the α1-helix, respectively (**Fig. 4a**). Here, the CDR3α loop acts as a peg that fills the notch between these two H-2D^b loops (**Fig. 4a**), where large charged side chains from H-2D^b stabilized the CDR3α loop via a network of polar and non-polar interactions. Namely, Trp113α wedged between the Arg75 and Arg79, Glu108α, salt-bridged to Arg79, while Ser112α hydrogen bonded to Glu18 and the Arg75 (**Fig. 4a**). These CDR3α loop mediated contacts were conserved between the NP1-B17 and NP2-B17 TCRs. While the CDR3α loop made substantial contact with the MHC-I molecule, it did not engage the peptide (**Table 2** and **Fig. 3a,b**). Conversely, the CDR3β loops of the NP1-B17 and NP2-B17 TCRs engaged the MHC-I via one (Leu110β) or two residues (Leu110β and Asp111β), respectively, and made no contacts with the peptide (**Fig. 4b** and

Table 2). Thus, the extent of involvement and role of the CDR3 loops in these TRBV17^{+} TCR-H-2D[b]-NP$_{366}$ complexes is in stark contrast to all the TCR-pMHC-I complexes observed to date (Rossjohn et al., 2015).

The CDR2β loop and the framework segment of the β-chain (FWβ) made the majority of the contacts with the MHC-I (**Fig. 4c,d**). Here, the CDR2β loop sat over the H-2D[b] α1-helix, where Tyr57β and Ile64β interacted with Gln72 and Gly69 & Trp73, respectively (**Fig. 4c**). A large stretch of 11 residues (66 to 77) from the FWβ region contacted both the α1- and α2-helices of the H-2D[b] molecule (**Fig. 4d** and **Table 2**). Here, the side chain of the Asn66β formed a hydrogen bond with Asn80, and van der Waals interaction with Val76 from the α1-helix (**Fig. 4c**), while the FWβ region interacted with a focused region (142-150) of the α2-helix (**Fig. 4d**). Prominently, Arg67β lay flat in a head-to-tail orientation on the top of Lys146 (**Fig. 4d**), with the positively charged head groups forming a hydrogen bond with their respective main chains. Collectively, the extent of interactions with the TCR β-chain provided insight into the TRBV17 bias, and very unusual interactions underpinned this reversed TCR-pMHC-I docking mode.

Germline-encoded recognition of the NP$_{366}$ peptide

In all of the TCR-pMHC-I structures solved to date, at least one of the non-germline encoded CDR3 loops is involved in contacting the peptide (Rossjohn et al., 2015). However, neither of the TRBV17^{+} TCR CDR3 loops contacted the NP$_{366}$ peptide. Instead, peptide contacts were mediated solely by the TCR β-chain germline-encoded residues (**Fig. 3a,b** and **Table 2**). Specifically, the CDR2β and FWβ region formed a "lid-like" structure with the C-terminal end of the peptide (Asn5-Thr8) (**Fig. 4e**). Here, Asn5 and Met6 formed main chain interactions with Ile64β from the CDR2β loop, while the aliphatic moiety of Glu7 packed against Leu65β from the CDR2β loop, and its carboxyl group salt-bridged to Arg67β from the FWβ region (**Fig. 4e**). Thr8 formed van der Waals interactions with Ile64β and Leu65β of the CDR2β loop, as well as hydrogen bonding to the main chain of the Leu65β and the side chain of the FWβ-Asn66. In addition, the small size of Thr8 permitted an intricate network of interactions between the TCR and the MHC (not shown). In summary, the TRBV17^{+} TCR engaged the peptide in an unprecedented manner, whereby the germline-encoded regions of the TRBV17 chain solely dictated peptide specificity.

TRBV17[+] TCR displays a large energetic footprint on H-2D[b]

We next established the energetic basis underpinning the NP1-B17 TCR interaction by a large alanine-scanning mutagenesis study. Based on the crystal structure, 22 mutant pMHC-I complexes were generated (15 H-2D[b] and 7 NP_{366} mutants) (**Table 1**) (Burrows et al., 2010). We first checked the thermal stability of the 23 pMHC-I complexes generated (**Supplemental Table 3**). The H-2D[b]-NP_{366} complex showed a thermal melting point (T_m) of ~50°C and all but two of the mutants (H-2D[b]-K146A (~41°C) and NP_{366} mutant A1N (~43°C)), were as stable as the H-2D[b]-NP_{366}, allowing us to assess the importance of each mutated position in mediating NP1-B17 TCR recognition.

The affinity of the NP1-B17 TCR, as measured by SPR, for each H-2D[b] or peptide mutant was compared to the H-2D[b]-NP_{366} WT, with the effect classified as negligible if the affinity was decreased by less than three-fold, moderate if the affinity decreased by three to five-fold, and critical ("hot spots") if the affinity changed by more than five-fold. As expected, the control triple mutation of MHC residues (positions 65, 69 and 155) (Burrows et al., 2010; Tynan et al., 2005) had no impact on NP1-B17 TCR recognition (**Fig. 5a** and **Table 1**). Of the other 14 H-2D[b] single site mutants tested, seven did not impact the NP1-B17 TCR affinity, three had a moderate impact and five were critical for the NP1-B17 TCR recognition (**Fig. 5a**, **Table 1** and **Supplemental Fig. 3**).

The hot spots were clustered at the C-terminal region of the antigen-binding cleft (Arg75, Val76, Arg79, Asn80 and Lys146), surrounded by the three moderately important amino acids (Glu18, Ala89, Gln149) (**Fig. 5a** and **Table 1**). Two of the moderate mutations (Glu18 and the Ala89) were located in the loops (14-21 and 85-92) (Rossjohn et al., 2015), thereby underpinning the importance of this atypical region in mediating NP1-B17 TCR contacts. Notably, Arg75 and Arg79 formed interactions with the CDR3α and CDR3β loops, while the FWβ region mediated 3 critical contacts with the H-2D[b] molecule; Asn80, Val76, and Lys146, (**Table 1** and **Fig. 5a**). Accordingly, the energetic footprint highlighted the critical contribution of the CDR3 loops in mediating interaction with the MHC molecule.

Peptide specificity of the reversed docking CD8^{+} TCR

Next we determined the extent to which the TCR was dependent on the NP_{366} peptide for recognition of the H-2D[b]-NP_{366} complex. Here, SPR analysis was performed using H-2D[b] loaded with unrelated peptide (namely $PA_{224-233}$, derived from the acid polymerase protein of IAV, or GAP50, derived from

the malaria *Pb*A glideosome-associated protein 50 (Gordon et al., 2015)), or with NP_{366} peptide mutants. Neither the $PA_{224-233}$ nor the GAP50 peptide bound to $H-2D^b$ showed any interaction with the NP1-B17 TCR, indicating that this interaction is peptide dependent. The Ala1 did not contact the NP1-B17 TCR, but had a moderate impact on TCR affinity (**Table 1**), which is likely an indirect consequence of decreased stability of the $H-2D^b$-NP_{366}-A1N (**Supplemental Table 3**). The mutation of the NP_{366} epitope at positions 3, 4 and 6 had no impact on NP1-B17 TCR affinity, despite being critical for recognition by polyclonal immune $H-2D^b$-NP_{366}-specific $CD8^+$ T cells (Turner et al., 2005). However, both Glu7Ala and Thr8Ala mutations dramatically decreased, by more than five-fold, the NP1-B17 TCR affinity (**Table 1**).

The Glu7 and the Thr8 residues of the NP_{366} epitope contacted the CDR2β and the FWβ regions of the NP1-B17 TCR (**Table 2**). The NP_{366} epitope hot spots were co-located with the $H-2D^b$ hot spots, thereby indicating that the C-terminal end of the antigen-binding cleft represented the focal point of the TCR interaction (**Fig. 5a**). Thus, despite the reversed docking mode adopted by the NP1-B17 $TRBV17^+$ TCR, and the lack of CDR3 loops interaction with peptide, it mediated a peptide-specific interaction.

$TRBV17^+$ TCR signaling corresponds to the affinity of the TCR-pMHC-I interaction

To support the contention that the reverse docking topology is responsible for the poor involvement of $TRBV17^+$ T cells in the IAV-specific immune response, we introduced 16 single alanine mutations in the NP1-B17 TCR (15 residues that contact the pMHC-I, and 1 control residue (Val59α) that does not contact the pMHC-I) (**Fig. 5b,c**). Upon transducing these 16 mutant TCRs into a Jurkat T cell line, we assessed the ability of the mutant TCRs to transduce a signal (via pERK1/2 staining) following specific recognition of $H-2D^b$-NP_{366}. The impact of mutation was classified as negligible if pERK1/2 staining was >60% of that observed with the WT NP1-B17 TCR staining; moderate if it fell between 10-60%; and critical if there was <10%. The control (Val59α) mutation had no effect on signaling (**Fig. 5b,c**). Three other TCR mutants, all belonging to the CDR3α loop (Glu108α, Gly111α and Gln114α), also had no impact on signaling. Five residues showed a moderate impact on T cell signaling, namely three from the CDR3α loop (Thr109α, Ser110α and Ser112α) and two from the FWβ region (Phe72β and Glu74β) (**Fig. 5b,c**). Notably, seven residues were critical for T cell signaling, as their alanine substitution abrogated the pERK1/2 response. The critical residues were Trp113α and Leu110β from the CDR3α and CDR3β loops respectively; Tyr57β, Ile64β and Leu65β from CDR2β; and the FWβ

11

residues Asn66β and Arg67β. All the critical TCR residues mediated interactions with the MHC and/or peptide, and there was a very close correlation between key peptide and MHC residues impacting on affinity of the interaction and the corresponding TCR residues impacting on T cell signaling. Moreover, all the TCR residues, namely Ile64β, Leu65β, Asn66β and Arg67β contacting the peptide were critical for T cell signaling (**Fig. 5b, c**). Collectively these data demonstrate that impacting the affinity of the TCR-pMHC-I interaction has a direct and corresponding impact on T cell signaling.

TRBV17^{+} T cells and MHC-restriction

Given the reversed polarity docking topology and the moderate affinity of the selected H-2D^b-NP$_{366}$ reactive TRBV17^{+} T cells, we investigated the possibility that these T cells depended on H-2K^b for positive selection in the thymus, and cross-reacted with H-2D^b-NP$_{366}$ in the periphery. Because ~25% of the H-2D^b-NP$_{366}$-specific repertoire is comprised of TRBV17^{+} T cells (Cukalac et al., 2015), the absence of H-2K^b would, in that case, result in a substantial reduction in both the number and TRBV17 usage of naïve H-2D^b-NP$_{366}$-specific cells. The H-2K^b-/- mice had a substantially larger proportion of CD8^{+} T cells compared to mice lacking both H-2K^b and H-2D^b, indicating that the vast majority of T cells present in H-2K^b-/- mice are selected on H-2D^b (**Fig. 5d**) (Perarnau et al., 1999). Both H-2K^b-/- and WT mice were equally capable of generating naïve H-2D^b-NP$_{366}$-specific CD8^{+} T cells (**Fig. 5e**), with similar TRBV17 usage by such cells in both strains (**Fig. 5f**). Thus, the H-2D^b-NP$_{366}$-specific TRBV17^{+} population is not dependent on H-2K^b for thymic development, and is most likely selected on H-2D^b.

Discussion

The factors that contribute to the recruitment and expansion of T cells from the naïve repertoire into the immune repertoire are complex and unclear. In some cases, even following infection, a subset of the epitope-specific naïve pool remains unrecruited (Coles et al., 2003; La Gruta et al., 2010; Malherbe et al., 2004; Obar et al., 2008). Moreover, direct comparison of TCR usage in naïve and immune epitope-specific T cell repertoires revealed that some T cells, whilst abundant in the naïve repertoire, are nevertheless greatly and reproducibly diminished in the immune repertoire upon viral challenge (Cukalac et al., 2015; Neller et al., 2015). These findings demonstrate that the extent of involvement of particular T cell clones in the immune response is selective. Here we provide mechanistic insight into this observation, revealing that a minimal contribution to the immune repertoire can correlate with a reversed TCR-pMHC-I docking topology.

The diminished prevalence of TRBV17^{+} T cells in the IAV-specific immune repertoire was not attributable to the TRBV17^{+} T cells being redistributed to a distinct tissue/organ or being selected on another restriction element. Moreover, the observation that the fold expansion of each Rg T cell population (TRBV13-1[+] or TRBV17^{+}) was reproducible, irrespective of whether they were transferred separately or together, or in the presence or absence of an endogenous IAV-specific CD8^{+} T cell response, indicates that the poor responsiveness of the TRBV17^{+} T cell population is intrinsic and unrelated to competition with other responding T cell populations. The reduced capacity of the TRBV17^{+} TCRs to contribute to the IAV-specific immune response is possibly due to the relative low avidity of the TRBV17^{+} T cells towards H-2D^b-NP$_{366}$ compared to that of the TRBV13-1[+] T cell population (Busch and Pamer, 1999; Cukalac et al., 2014; McHeyzer-Williams et al., 1999; Price et al., 2005). Mutational analyses demonstrated that the relative impact of disrupting TCR-pMHC-I affinity, correlated with the extent of impact on T cell signaling. Thus, the nature of the reversed TCR-pMHC-I interaction drives, in part, the efficiency (or lack thereof) of signaling and therefore activation.

Another aspect by which a reversed TCR-pMHC-I docking topology may result in poor activation of T cells centers on our understanding of the structural organization of the TCR/pMHC/co-receptor complex (Yin et al., 2012) and the CD3 docking site on TCRβ (Birnbaum et al., 2014; He et al., 2015). Here, the CD3 complex is located within an arch-like structure on the T cell surface and is thus co-localized with both TCRαβ and co-receptor-associated Lck, facilitating the phosphorylation of CD3 ITAMs (He et al., 2015; Rangarajan and Mariuzza, 2014; Yin et al., 2012). Accordingly, a reversed TCR docking polarity would place the CD3 complex outside of the arch, thereby reducing its proximity

to Lck and consequently the efficiency of ITAM phosphorylation (Rangarajan and Mariuzza, 2014; Yin et al., 2012). While the quaternary TCR/pMHC-I/CD8 complex structure has not been solved, a similar structural organization likely applies for CD8^{+} T cells (Yin et al., 2012). In this way the reverse docking topology may negatively impact the efficiency of signaling independently of TCR-pMHC-I affinity. In summary, the associated functionality of the TRBV17^{+} T cells were inferior to that of the TRBV13-1^{+} T cells, implying that this is related to the way in which TRBV17^{+} TCRs engaged the pMHC-I.

In MHC-restricted immunity, the TCR has universally (with one prominent exception (Beringer et al., 2015)) adopted a consensus polarity above the MHC. This consistent polarity of the TCR-pMHC docking mode has been the key argument pertaining to TCRs being hard-wired to interact with the MHC (the germline-encoded model) (Garcia et al., 2009). An extension to this TCR hard-wiring concept is the "interaction codon hypothesis" pertaining to TCR-pMHC interactions, which posits that conserved pairwise interaction motifs between the germline-encoded regions of the TCR and the MHC underpin this TCR-MHC co-evolution (Adams et al., 2016). In contrast to the germline model, the selection model argues that MHC restriction is not an intrinsic feature of TCRs but is conferred by selection events in the thymus (Holland et al., 2012; Van Laethem et al., 2013). Here we show that the two TRBV17^{+} TCRs, which are found within the naïve T cell repertoire in wild type mice, adopt a reversed TCR-pMHC-I docking topology. Moreover, within this reversed TCR-pMHC-I framework, the non-germline-encoded CDR3 loops exclusively contacted the MHC-I molecule. It is difficult to reconcile these structural features of a naturally selected TCR, as well as that recently observed in the TCR-pMHC-II setting (Beringer et al., 2015), within the framework of the germline-encoded model of TCR recognition.

Alternatively, the fact that such variations on the consensus docking mode have not been seen in the TCR-pMHC-I structures solved to date, as well as our current demonstration of the relative inability of a variant docking mode to support efficient immune selection, may suggest that this non-canonical docking mode is the exception that proves the rule of germline selection. However, this is the first ternary complex structure of antigen-specific TCRs from the *naïve* repertoire and so the frequency of unconventionally docked TCRs in this pool is unknown. It is possible that thymic selection permits a much broader range of TCR-pMHC interactions – the signaling threshold for thymic selection is lower than that required for peripheral T cell activation (Davey et al., 1998; Hogquist et al., 1994) - and that the infrequency of unconventional TCR-pMHC recognition in immune repertoires reflects a further

'selection' event beyond thymic selection. Resolution of further naïve TCR-pMHC structures is therefore essential.

Our observation clearly resonates with the recently described reversed polarity observed in a TCR-pMHC-II setting (Beringer et al., 2015). While the MHC-II restricted TCR originated from the naïve T cell repertoire, it was nevertheless isolated from an induced Treg cell, and the reversed docking mode was suggested to be a mechanism related to Treg fate (Beringer et al., 2015). We now show that reversed TCR docking can also be a salient determinant of why certain T cells, whilst abundant in the naïve repertoire, are not selected into the immune repertoire. This would also explain why this docking mode has not been observed in previous structural analyses, which have focused on TCRs identified from immune populations. These findings demonstrate that the naïve CD4^{+} and CD8^{+} T cell repertoire expresses TCRs that can latch onto the MHC in reversed polarity docking modes. Together with the reports that TCRs can ligate non-MHC molecules in co-receptor deficient mice (Tikhonova et al., 2012; Van Laethem et al., 2007) or mice in which Lck is freed from the CD4 and CD8 co-receptors (Van Laethem et al., 2013), it suggests that TCRs can bind the MHC in a number of distinct modes that are neither limited to docking geometries or signaling constraints. However, here we demonstrate that the reversed TCR-pMHC-I docking is coincident with a diminished contribution to the immune repertoire.

Experimental Procedures

Mice and virus infection

Female C57BL/6J (H-2^b) WT, H-2K^b-/-, H-2K^b/D^b-/- (Perarnau et al., 1999), OTI TCR transgenic, RAG1-/-, and TCRα-/- mice were bred and housed in the animal facility of the Department of Microbiology and Immunology, University of Melbourne (Parkville, Australia). Naïve 6-10 week-old mice were infected i.n. with 1 x 10^4 PFU of HKx31 (H3N2) influenza A virus (La Gruta et al., 2004). All animal experimentation was reviewed and approved by the University of Melbourne Animal Ethics Committee.

Tetramer and antibody staining

Enriched single cell suspensions from mLN, spleen, and BAL from mice at d10 after primary IAV infection were stained with PE- or APC-conjugated tetrameric complexes of H-2D^b MHC class I glycoprotein loaded with nucleoprotein-derived NP$_{366–374}$ (ASNENMETM) (ImmunoID, University of Melbourne), along with fluorescently conjugated antibodies to CD8α, and either anti-Vβ9 (TRBV17) or anti-Vβ8.3 (TRBV13-1), as described (Cukalac et al., 2015).

In vitro TCR expression

293T cells were transfected with a bicistronic mouse stem cell virus (MSCV)-based retroviral vector containing αβTCR sequence with IRES-GFP (pMIGII) or IRES-mCherry (pMImC), as well as pMIGII encoding the CD3γδε and ζ subunits (Szymczak et al., 2004). Transfected 293T cells were labelled with H-2D^b-NP$_{366}$-APC tetramer 48 h later, followed by fluorescently conjugated anti-CD3ε and anti-TCRβ Abs. Alternatively, Jurkat-76 (Jurkat) cells were stably transduced with pMIGII retrovirus (Szymczak et al., 2004) encoding one of 16 mutant NP1-B17 TCRs (**Fig. 5** and **Table 2**).

Generation of retrogenic mice and adoptive transfer

Retrogenic mice expressing either the NP1-B17 or NP1-B13 TCRs were generated according to a published protocol (Holst et al., 2006), using bone marrow cells from RAG1-/- mice. Bone marrow reconstitution was verified by analysis of blood leucocytes ~6 weeks post-transplant. NP1-B17 or NP1-B13 Rg T cells (2.5 x 10^3) from pooled spleen and lymph nodes (sorted on the basis of CD8, CD3, and either GFP or mCherry co-expression) were transferred either separately or together into recipient WT, RAG1-/- or OTI TCR transgenic mice, followed by i.n. infection with IAV.

Magnetic enrichment of naïve epitope-specific CD8$^+$ T cells

Tetramer-based magnetic enrichment was used for identification of naïve epitope-specific CTLps in WT B6 and H-2K^b-/- mice, as described in detail previously (La Gruta et al., 2010; Moon et al., 2007; Obar et al., 2008). Entire samples were acquired on a FACSAria III cell sorter with FACSDiva software (BD Immunocytometry Systems, San Jose, CA, USA).

Intracellular cytokine staining

Mice that had received Rg CD8$^+$ T cells were administered i.n. with IAV the following day and then spleen and BAL were harvested at d10 post-infection. Enriched cell populations were then incubated with or without NP$_{366}$ peptide (1μM) at 37°C, 5% CO2 for 5h, before surface staining with fluorescently labelled anti-CD8α followed by permeabilization, fixation and intracellular staining for IFN-γ, TNF, and IL-2 using BD Cytofix/Cytoperm kit (La Gruta et al., 2004).

T cell signaling

Peptide pulsed bone marrow derived dendritic cells (BMDCs) and DC2.4 cells (provided as a kind gift from Professor Kenneth Rock, University of Massachusetts Medical School) were incubated with GFP+ retrogenic NP1-B17 or NP1-B13 cells or Jurkat transductants expressing NP1-B17 wt or mutant TCRs, respectively. Cells were spun together to allow conjugation for the indicated timepoints, stained for pERK1/2 expression, and analyzed by flow cytometry. For more details see **Supplemental Experimental Procedures**.

Protein expression, purification, crystallisation and structure determination

The NP1-B17 and NP2-B17 TCRs as well as the wt and mutants pMHC complex were expressed, refolded and purified as previously described (Day et al., 2011). Further details are included in **Supplemental Experimental Procedures**.

Thermal stability assay

To assess the effect of each mutation on the pMHC complex stability, a thermal shift assay was performed using fluorescent dye Sypro orange to monitor the protein unfolding as previously described (Gras et al., 2012). Results are reported in **Supplemental Table 3**.

Surface Plasmon Resonance Measurement and Analysis

All surface plasmon resonance experiments were conducted at 25°C on the BIAcore 3000 instrument

with 10mM Tris-HCl, pH 8, 150mM NaCl, 0.005% surfactant P20 and 1% BSA buffer. The NP1-B17 and NP2-B17 TCRs, as well as a negative control (LC13 (Gras et al., 2009)), bound to a CM5 sensor chip via amine coupling, and the pMHC was flown over the TCRs with a maximum concentration of 0.78-200 µM. The experiment was conducted as previously described (Gras et al., 2009) in duplicate with n=2. BIAevaluation Version 3.1 was used for data analysis with the 1:1 Langmuir binding model, the results are summarized in **Table 1**.

Author Contributions

Conceptualization: S.G., N.L.L.G., J.R.; Investigation: S.G., J.C., C.M.D.C., C.F., F.W., T.M.J., X.Y.X.S., M.M., K.A.W., K.M.Q.; Funding acquisition: S.G., N.L.L.G., J.R.; Supervision: N.L.L.G., J.R., T.T.; Writing – Original Draft: N.L.L.G., J.R., S.G.; Writing – Review and Editing: N.L.L.G., J.R., S.G., J.C., K.M.Q., T.M.J., K.A.W.

References

Adams, J.J., Narayanan, S., Birnbaum, M.E., Sidhu, S.S., Blevins, S.J., Gee, M.H., Sibener, L.V., Baker, B.M., Kranz, D.M., and Garcia, K.C. (2016). Structural interplay between germline interactions and adaptive recognition determines the bandwidth of TCR-peptide-MHC cross-reactivity. Nat. Immunol. *17*, 87-94.

Beringer, D.X., Kleijwegt, F.S., Wiede, F., van der Slik, A.R., Loh, K.L., Petersen, J., Dudek, N.L., Duinkerken, G., Laban, S., Joosten, A*., et al.* (2015). T cell receptor reversed polarity recognition of a self-antigen major histocompatibility complex. Nat. Immunol. *16*, 1153-1161.

Birnbaum, M.E., Berry, R., Hsiao, Y.S., Chen, Z., Shingu-Vazquez, M.A., Yu, X., Waghray, D., Fischer, S., McCluskey, J., Rossjohn, J*., et al.* (2014). Molecular architecture of the alphabeta T cell receptor-CD3 complex. Proc Natl Acad Sci U S A *111*, 17576-17581.

Bricogne G., B.E., Brandl M., Flensburg C., Keller P., Paciorek W.,, and Roversi P, S.A., Smart O.S., Vonrhein C., Womack T.O. (2011). Buster version 2.10. Cambridge, United Kingdom: Global Phasing Ltd.

Burrows, S.R., Chen, Z., Archbold, J.K., Tynan, F.E., Beddoe, T., Kjer-Nielsen, L., Miles, J.J., Khanna, R., Moss, D.J., Liu, Y.C*., et al.* (2010). Hard wiring of T cell receptor specificity for the major histocompatibility complex is underpinned by TCR adaptability. Proc Natl Acad Sci U S A *107*, 10608-10613.

Busch, D.H., and Pamer, E.G. (1999). T cell affinity maturation by selective expansion during infection. J. Exp. Med. *189*, 701-710.

Chen, H., Ndhlovu, Z.M., Liu, D., Porter, L.C., Fang, J.W., Darko, S., Brockman, M.A., Miura, T., Brumme, Z.L., Schneidewind, A*., et al.* (2012). TCR clonotypes modulate the protective effect of HLA class I molecules in HIV-1 infection. Nat. Immunol. *13*, 691-700.

Coles, R.M., Jones, C.M., Brooks, A.G., Cameron, P.U., Heath, W.R., and Carbone, F.R. (2003). Virus infection expands a biased subset of T cells that bind tetrameric class I peptide complexes. Eur. J. Immunol. *33*, 1557-1567.

Cukalac, T., Chadderton, J., Handel, A., Doherty, P.C., Turner, S.J., Thomas, P.G., and La Gruta, N.L. (2014). Reproducible selection of high avidity CD8+ T-cell clones following secondary acute virus infection. Proc Natl Acad Sci U S A *111*, 1485-1490.

Cukalac, T., Kan, W.T., Dash, P., Guan, J., Quinn, K.M., Gras, S., Thomas, P.G., and La Gruta, N.L. (2015). Paired TCRalphabeta analysis of virus-specific CD8 T cells exposes diversity in a previously defined 'narrow' repertoire. Immunol. Cell. Biol. *93*, 804-814.

Davey, G.M., Schober, S.L., Endrizzi, B.T., Dutcher, A.K., Jameson, S.C., and Hogquist, K.A. (1998). Preselection thymocytes are more sensitive to T cell receptor stimulation than mature T cells. J. Exp. Med. *188*, 1867-1874.

Davis, M.M., and Bjorkman, P.J. (1988). T-cell antigen receptor genes and T-cell recognition. Nature *334*, 395-402.

Day, E.B., Guillonneau, C., Gras, S., La Gruta, N.L., Vignali, D.A., Doherty, P.C., Purcell, A.W., Rossjohn, J., and Turner, S.J. (2011). Structural basis for enabling T-cell receptor diversity within biased virus-specific CD8+ T-cell responses. Proc Natl Acad Sci U S A *108*, 9536-9541.

Deckhut, A.M., Allan, W., McMickle, A., Eichelberger, M., Blackman, M.A., Doherty, P.C., and Woodland, D.L. (1993). Prominent usage of V beta 8.3 T cells in the H-2Db-restricted response to an

influenza A virus nucleoprotein epitope. J. Immunol. *151*, 2658-2666.

DeLano, W.L. (2002). The PyMOL Molecular Graphics System.

Dong, T., Stewart-Jones, G., Chen, N., Easterbrook, P., Xu, X., Papagno, L., Appay, V., Weekes, M., Conlon, C., Spina, C*., et al.* (2004). HIV-specific cytotoxic T cells from long-term survivors select a unique T cell receptor. The Journal of experimental medicine *200*, 1547-1557.

Emsley, P., and Cowtan, K. (2004). Coot: model-building tools for molecular graphics. Acta Crystallogr D Biol Crystallogr *60*, 2126-2132.

Evans, P. (2006). Scaling and assessment of data quality. Acta Crystallogr D Biol Crystallogr *62*, 72-82.

Garcia, K.C., Adams, J.J., Feng, D., and Ely, L.K. (2009). The molecular basis of TCR germline bias for MHC is surprisingly simple. Nat. Immunol. *10*, 143-147.

Gordon, E.B., Hart, G.T., Tran, T.M., Waisberg, M., Akkaya, M., Kim, A.S., Hamilton, S.E., Pena, M., Yazew, T., Qi, C.F*., et al.* (2015). Targeting glutamine metabolism rescues mice from late-stage cerebral malaria. Proc Natl Acad Sci U S A *112*, 13075-13080.

Gras, S., Burrows, S.R., Kjer-Nielsen, L., Clements, C.S., Liu, Y.C., Sullivan, L.C., Bell, M.J., Brooks, A.G., Purcell, A.W., McCluskey, J., and Rossjohn, J. (2009). The Shaping of T Cell Receptor Recognition by Self-Tolerance. Immunity *30*, 193-203.

Gras, S., Wilmann, P.G., Chen, Z., Halim, H., Liu, Y.C., Kjer-Nielsen, L., Purcell, A.W., Burrows, S.R., McCluskey, J., and Rossjohn, J. (2012). A structural basis for varied alphabeta TCR usage against an immunodominant EBV antigen restricted to a HLA-B8 molecule. J. Immunol. *188*, 311-321.

He, Y., Rangarajan, S., Kerzic, M., Luo, M., Chen, Y., Wang, Q., Yin, Y., Workman, C.J., Vignali, K.M., Vignali, D.A*., et al.* (2015). Identification of the Docking Site for CD3 on the T Cell Receptor beta Chain by Solution NMR. J. Biol. Chem. *290*, 19796-19805.

Hogquist, K.A., Jameson, S.C., Heath, W.R., Howard, J.L., Bevan, M.J., and Carbone, F.R. (1994). T cell receptor antagonist peptides induce positive selection. Cell *76*, 17-27.

Holland, S.J., Bartok, I., Attaf, M., Genolet, R., Luescher, I.F., Kotsiou, E., Richard, A., Wang, E., White, M., Coe, D.J*., et al.* (2012). The T-cell receptor is not hardwired to engage MHC ligands. Proc Natl Acad Sci U S A *109*, E3111-3118.

Holst, J., Szymczak-Workman, A.L., Vignali, K.M., Burton, A.R., Workman, C.J., and Vignali, D.A. (2006). Generation of T-cell receptor retrogenic mice. Nat Protoc *1*, 406-417.

Kjer-Nielsen, L., Clements, C.S., Brooks, A.G., Purcell, A.W., McCluskey, J., and Rossjohn, J. (2002). The 1.5 A crystal structure of a highly selected antiviral T cell receptor provides evidence for a structural basis of immunodominance. Structure *10*, 1521-1532.

Kjer-Nielsen, L., Clements, C.S., Purcell, A.W., Brooks, A.G., Whisstock, J.C., Burrows, S.R., McCluskey, J., and Rossjohn, J. (2003). A structural basis for the selection of dominant alphabeta T cell receptors in antiviral immunity. Immunity *18*, 53-64.

La Gruta, N.L., Rothwell, W.T., Cukalac, T., Swan, N.G., Valkenburg, S.A., Kedzierska, K., Thomas, P.G., Doherty, P.C., and Turner, S.J. (2010). Primary CTL response magnitude in mice is determined by the extent of naive T cell recruitment and subsequent clonal expansion. J. Clin. Invest. *120*, 1885-1894.

La Gruta, N.L., Turner, S.J., and Doherty, P.C. (2004). Hierarchies in cytokine expression profiles for acute and resolving influenza virus-specific CD8+ T cell responses: correlation of cytokine profile and

TCR avidity. J. Immunol. *172*, 5553-5560.

Lefranc, M.P. (2003). IMGT databases, web resources and tools for immunoglobulin and T cell receptor sequence analysis, http://imgt.cines.fr. Leukemia *17*, 260-266.

Leslie, A.G.W. (1992). Recent changes to the MOSFLM package for processing film and image plate data. Joint CCP4 + ESF-EAMCB Newsletter on Protein Crystallography *26*.

Malherbe, L., Hausl, C., Teyton, L., and McHeyzer-Williams, M.G. (2004). Clonal selection of helper T cells is determined by an affinity threshold with no further skewing of TCR binding properties. Immunity *21*, 669-679.

McHeyzer-Williams, L.J., Panus, J.F., Mikszta, J.A., and McHeyzer-Williams, M.G. (1999). Evolution of antigen-specific T cell receptors in vivo: preimmune and antigen-driven selection of preferred complementarity-determining region 3 (CDR3) motifs. J. Exp. Med. *189*, 1823-1838.

Miles, J.J., Douek, D.C., and Price, D.A. (2011). Bias in the alphabeta T-cell repertoire: implications for disease pathogenesis and vaccination. Immunol. Cell Biol. *89*, 375-387.

Moon, J.J., Chu, H.H., Pepper, M., McSorley, S.J., Jameson, S.C., Kedl, R.M., and Jenkins, M.K. (2007). Naive CD4(+) T cell frequency varies for different epitopes and predicts repertoire diversity and response magnitude. Immunity *27*, 203-213.

Neller, M.A., Ladell, K., McLaren, J.E., Matthews, K.K., Gostick, E., Pentier, J.M., Dolton, G., Schauenburg, A.J., Koning, D., Fontaine Costa, A.I*., et al.* (2015). Naive CD8(+) T-cell precursors display structured TCR repertoires and composite antigen-driven selection dynamics. Immunol. Cell Biol. *93*, 625-633.

Obar, J.J., Khanna, K.M., and Lefrancois, L. (2008). Endogenous naive CD8+ T cell precursor frequency regulates primary and memory responses to infection. Immunity *28*, 859-869.

Pace, L., Tempez, A., Arnold-Schrauf, C., Lemaitre, F., Bousso, P., Fetler, L., Sparwasser, T., and Amigorena, S. (2012). Regulatory T cells increase the avidity of primary CD8+ T cell responses and promote memory. Science *338*, 532-536.

Perarnau, B., Saron, M.F., Reina San Martin, B., Bervas, N., Ong, H., Soloski, M.J., Smith, A.G., Ure, J.M., Gairin, J.E., and Lemonnier, F.A. (1999). Single H2Kb, H2Db and double H2KbDb knockout mice: peripheral CD8+ T cell repertoire and anti-lymphocytic choriomeningitis virus cytolytic responses. Eur. J. Immunol. *29*, 1243-1252.

Price, D.A., Brenchley, J.M., Ruff, L.E., Betts, M.R., Hill, B.J., Roederer, M., Koup, R.A., Migueles, S.A., Gostick, E., Wooldridge, L*., et al.* (2005). Avidity for antigen shapes clonal dominance in CD8+ T cell populations specific for persistent DNA viruses. J. Exp. Med. *202*, 1349-1361.

Rangarajan, S., and Mariuzza, R.A. (2014). T cell receptor bias for MHC: co-evolution or co-receptors? Cell. Mol. Life Sci. *71*, 3059-3068.

Read, R.J. (2001). Pushing the boundaries of molecular replacement with maximum likelihood. Acta Crystallogr D Biol Crystallogr *57*, 1373-1382.

Rossjohn, J., Gras, S., Miles, J.J., Turner, S.J., Godfrey, D.I., and McCluskey, J. (2015). T cell antigen receptor recognition of antigen-presenting molecules. Annu. Rev. Immunol. *33*, 169-200.

Seder, R.A., Darrah, P.A., and Roederer, M. (2008). T-cell quality in memory and protection: implications for vaccine design. Nat. Rev. Immunol. *8*, 247-258.

Szymczak, A.L., Workman, C.J., Wang, Y., Vignali, K.M., Dilioglou, S., Vanin, E.F., and Vignali, D.A. (2004). Correction of multi-gene deficiency in vivo using a single 'self-cleaving' 2A peptide-

based retroviral vector. Nat. Biotechnol. *22*, 589-594.

Tikhonova, A.N., Van Laethem, F., Hanada, K., Lu, J., Pobezinsky, L.A., Hong, C., Guinter, T.I., Jeurling, S.K., Bernhardt, G., Park, J.H.*, et al.* (2012). alphabeta T cell receptors that do not undergo major histocompatibility complex-specific thymic selection possess antibody-like recognition specificities. Immunity *36*, 79-91.

Townsend, A.R., Rothbard, J., Gotch, F.M., Bahadur, G., Wraith, D., and McMichael, A.J. (1986). The epitopes of influenza nucleoprotein recognized by cytotoxic T lymphocytes can be defined with short synthetic peptides. Cell *44*, 959-968.

Turner, S.J., Doherty, P.C., McCluskey, J., and Rossjohn, J. (2006). Structural determinants of T-cell receptor bias in immunity. Nat. Rev. Immunol. *6*, 883-894.

Turner, S.J., Kedzierska, K., Komodromou, H., La Gruta, N.L., Dunstone, M.A., Webb, A.I., Webby, R., Walden, H., Xie, W., McCluskey, J.*, et al.* (2005). Lack of prominent peptide-major histocompatibility complex features limits repertoire diversity in virus-specific CD8+ T cell populations. Nat. Immunol. *6*, 382-389.

Tynan, F.E., Burrows, S.R., Buckle, A.M., Clements, C.S., Borg, N.A., Miles, J.J., Beddoe, T., Whisstock, J.C., Wilce, M.C., Silins, S.L.*, et al.* (2005). T cell receptor recognition of a 'super-bulged' major histocompatibility complex class I-bound peptide. Nat. Immunol. *6*, 1114-1122.

Valkenburg, S.A., Gras, S., Guillonneau, C., Hatton, L.A., Bird, N.A., Twist, K.A., Halim, H., Jackson, D.C., Purcell, A.W., Turner, S.J.*, et al.* (2013). Preemptive priming readily overcomes structure-based mechanisms of virus escape. Proc Natl Acad Sci U S A *110*, 5570-5575.

van Heijst, J.W., Gerlach, C., Swart, E., Sie, D., Nunes-Alves, C., Kerkhoven, R.M., Arens, R., Correia-Neves, M., Schepers, K., and Schumacher, T.N. (2009). Recruitment of antigen-specific CD8+ T cells in response to infection is markedly efficient. Science *325*, 1265-1269.

Van Laethem, F., Sarafova, S.D., Park, J.H., Tai, X., Pobezinsky, L., Guinter, T.I., Adoro, S., Adams, A., Sharrow, S.O., Feigenbaum, L., and Singer, A. (2007). Deletion of CD4 and CD8 coreceptors permits generation of alphabetaT cells that recognize antigens independently of the MHC. Immunity *27*, 735-750.

Van Laethem, F., Tikhonova, A.N., Pobezinsky, L.A., Tai, X., Kimura, M.Y., Le Saout, C., Guinter, T.I., Adams, A., Sharrow, S.O., Bernhardt, G.*, et al.* (2013). Lck availability during thymic selection determines the recognition specificity of the T cell repertoire. Cell *154*, 1326-1341.

Vivian, J.P., Duncan, R.C., Berry, R., O'Connor, G.M., Reid, H.H., Beddoe, T., Gras, S., Saunders, P.M., Olshina, M.A., Widjaja, J.M.*, et al.* (2011). Killer cell immunoglobulin-like receptor 3DL1-mediated recognition of human leukocyte antigen B. Nature *479*, 401-405.

Winn, M.D., Ballard, C.C., Cowtan, K.D., Dodson, E.J., Emsley, P., Evans, P.R., Keegan, R.M., Krissinel, E.B., Leslie, A.G., McCoy, A.*, et al.* (2011). Overview of the CCP4 suite and current developments. Acta Crystallogr D Biol Crystallogr *67*, 235-242.

Yin, Y., Wang, X.X., and Mariuzza, R.A. (2012). Crystal structure of a complete ternary complex of T-cell receptor, peptide-MHC, and CD4. Proc Natl Acad Sci U S A *109*, 5405-5410.

Zehn, D., Lee, S.Y., and Bevan, M.J. (2009). Complete but curtailed T-cell response to very low-affinity antigen. Nature *458*, 211-214.

Figure Legends

Figure 1. TRBV17$^+$ T cells contribute minimally to the H-2D^b-NP$_{366}$-specific anti-viral response and exhibit reduced affinity. (**a**) Flow cytometric dot plots showing the proportion of CD8$^+$ T cells recovered from BAL at d10 after i.n. IAV infection that are tetramer$^+$ (left) and the proportion of tetramer$^+$ CD8$^+$ T cells that are TRBV$^+$ (right). (**b**) Percentage of the H-2D^b-NP$_{366}$-specific CTL response using TRBV17 or TRBV13-1 TCRs in the mLN, spleen and BAL at d7 or d10 after IAV infection. (**c**) Tetramer MFI on TRBV17$^+$ or TRBV13-1$^+$ H-2D^b-NP$_{366}$-specific CTLs at d10 after IAV infection. Shown are data points from 9 individual mice and the mean +/- standard deviation. *p<0.05, **p<0.01, ***p<0.001, ****p<0.0001 using Student's paired t test for (**b**) and (**c**). (**d**) At 48h after transfection of 293T cells with vectors encoding the designated TCRαβ and CD3γδε and ζ, cells expressing no TCR (black), intermediate TCR (open grey) or high TCR (dashed, grey fill) levels were analyzed for levels of tetramer staining. (**e**) H-2D^b-NP$_{366}$ tetramer MFI was determined for five different TRBV13-1 TCRs and two TRBV17 TCRs at each of the stated levels of TCR. Data is representative of 2 independent experiments. (**f**) Binding response of NP1-B17 (LHS) and NP2-B17 (RHS) TCRs against H-2D^b-NP$_{366}$ complex as analyte. The SPR sensograms represent the binding of a concentration range of H-2D^b-NP$_{366}$ (0.78-200 μM), from a single experiment, with the standard error of the mean represented (n=2). (**g**) CD8$^+$ T cells from blood of naïve NP1-B17 or NP1-B13 Rg mice were stained with H-2D^b-NP$_{366}$ tetramer and the levels of tetramer staining on GFP$^+$ cells (expressing equivalent TCR) from 8 individual Rg mice are shown.

Figure 2. Diminished expansion and function of adoptively transferred TRBV17$^+$ Rg cells after IAV infection. (**a**) NP1-B17 and NP1-B13 CD8$^+$ Rg cells (2,500 cells), identified by GFP or mCherry expression in 8-12 week old Rg mice, were adoptively transferred either separately or in combination into recipient WT B6 mice and mice were infected i.n. with IAV the following day. (**b**) Rg cells shown as a proportion of the total CD8 population in mLN, spleen and BAL at d10 after IAV infection, and fold expansion in the spleen relative to input number. (**c**) Cells recovered from spleen and BAL at d10 following IAV infection were stimulated *in vitro* for 5h with NP$_{366}$ peptide and IFN-γ, TNF, and IL-2 production determined by ICS. Shown are results from mice receiving either NP1-B17 or NP1-B13 cells. 3 mice/group for (b), 5 mice/group for (c) (**d**) NP1-B17 or NP1-B13 CD8$^+$ Rg cells were incubated with BMDCs pulsed with or without NP$_{366}$ peptide, or were incubated with anti-CD3ε Ab. Cells were removed after stimulation for either 10 or 45 min and phosphorylated ERK1/2 was stained with a fluorescently conjugated Ab and detected by flow cytometry (representative plots for each

treatment condition are shown). For all panels, *p<0.05, **p<0.01, ***p<0.001, ****p<0.0001 using Student's unpaired t-test (single transfer) or paired t-test (co-transfer), bars +/- error represent mean +/- SD, and all data is representative of 2 independent experiments.

Figure 3. Reversed docking polarity of NP1-B17 and NP2-B17 TCRs. The top panels represent the overall TCR-pMHC complex of (**a**) NP1-B17 TCR-H-2D^b-NP$_{366}$, (**b**) NP2-B17 TCR-H-2D^b-NP$_{366}$, (**c**) LC13-HLA-B8-FLR (Kjer-Nielsen et al., 2003) and (**d**) FS18-HLA-DR4-CL19 (Beringer et al., 2015). The TCRα chain is in light pink, the TCRβ chain is in pale blue, the H-2D^b is represented in white cartoon, HLA-B8; pale cyan, HLA-DR4; yellow and pale orange for the β- and α-chain, respectively, and peptide; black stick. The bottom panels represent the TCR atomic footprints on the surface of each corresponding pMHC complex (MHC; white surface, and peptide; grey surface). The pie charts represent the relative contributions of each TCR segment to the interaction with each pMHC complex. The CDR1, 2 and 3 loops are coloured in teal, green and purple for the α-chain, in red, orange and yellow for the β-chain. Contact with the framework (FW) is coloured in magenta for the FWα and dark blue for the FWβ, and the spheres represent the centre of mass of Vα and Vβ, in pink and blue, respectively. The docking angle of each TCR-pMHC complex is depicted next to the footprint. The dashed circle highlights the unique section of MHC-I contacted by the NP1-B17 and NP2-B17 TCRs (residue 14-21 and 85-92).

Figure 4. NP1-B17 TCR contacts with H-2D^b-NP$_{366}$. (**a**) Top view of the CDR3α loop (purple) interaction with H-2D^b (white). The two loops outside the antigen-binding cleft of H-2D^b are colored in black (residue 14-21 and 85-92). (**b**) Side view of the CDR3β loop (yellow) interaction with the H-2D^b. (**c, d**). Interactions of the CDR2β (orange) and FWβ (pale blue) with H-2D^b. The sphere represents Gly69. (**e**) NP1-B17 TCR interaction with the peptide (black stick) via the CDR2β (orange) and the FWβ segment. Blue and red dashed lines represent hydrophobic and polar interactions, respectively.

Figure 5. TRBV17$^+$ TCRs show a correlation between affinity and signal strength, and undergo thymic selection on H-2D^b molecule. (**a**) Surface representation of the H-2D^b (white) and sphere representation of NP$_{366}$ (pale cyan) complex. The colour depicts the impact of the pMHC-I residue on the NP1-B17 TCR binding, with black for no effect (<3-times the WT value), orange for a moderate effect (3 - 5-fold the WT value) and red for a critical effect (>5-times the WT value). (**b**) Surface representation of the NP1-B17 TCR (coloured in pale pink and blue for the α- and β-chains, respectively). The view is of the TCR-pMHC complex open in half (like a cut apple) showing the key

residues involved in the interaction. TCR residues have been color-coded according to the data in (**c**); green - mutants that improve signaling, dark grey - mutants that show >60% of pERK1/2 staining obtained with WT TCR (no impact), orange, mutants that show 10-60% of WT pERK1/2 staining (moderate impact), red - mutants that ablate signaling (<10%) (critical). (**c**) pERK1/2 staining in Jurkat TCR transductants expressing NP1-B17 TCR mutants containing single alanine substitutions, expressed relative to that induced by WT TCR. The bars are colored accordingly to the TCR segment to which each mutated residue belong, namely teal (CDR2α), purple (CDR3α), orange (CDR2β), blue (FWβ), yellow (CDR3β) or black for the WT TCR. The orange and red dashed lines represent 60 and 10%, respectively, of the pERK1/2 staining compare to WT TCR staining. Data are representative of 2 independent experiments. (**d**) Frequency of CD8$^+$ T cells from pooled spleen and lymph nodes of B6 WT, H-2K^b-/- and H-2K^b/D^b-/- mice. Using tetramer-based naïve enrichment with the H-2D^b-NP$_{366}$ tetramer, (**e**) the number of naïve H-2D^b-NP$_{366}$-specific CD8$^+$ T cells recovered from individual B6 WT and H-2K^b-/- mice and (**f**) the percentage of naïve H-2D^b-NP$_{366}$-specific CD8$^+$ T cells expressing TRBV17 was determined. * p<0.02, ****p<0.001, using a Mann-Whitney test. n=10-12 from 3 pooled experiments.

Table 1. NP1-B17 TCR affinity for H-2D^b-NP$_{366}$ and mutants

H-2D^b-NP$_{366}$	K$_{deq}$ (μM)	ΔΔG$_{eq}$ (kcal/mol)	Effect on affinity
WT	39.8 ± 4.5		
Mutant H-2D^b with NP$_{366}$	**K$_{deq}$ (μM)**	**ΔΔG$_{eq}$ (kcal/mol)**	**Effect on affinity**
E18A	133 ± 10	0.71	**
E19A	29.7 ± 0.9	-0.17	*
Q65A	66.7 ± 0.8	0.30	*
K68A	92.4 ± 1.0	0.49	*
Q72A	52.5 ± 4.2	0.16	*
R75A	NB	>> 0.95	***
V76A	> 200	> 0.95	***
R79A	> 200	> 0.95	***
N80A	NB	>> 0.95	***
A89V	135.5 ± 7.5	0.72	**
K146A	> 200	> 0.95	***
Q149A	175 ± 5	0.87	**
E163A	59.8 ± 6.2	0.24	*
H155A	76.4 ± 2.2	0.38	*
Q65A-G69A-H155A	82.5 ± 1.1	0.43	*
H-2D^b with mutant NP$_{366}$	**K$_{deq}$ (μM)**	**ΔΔG$_{eq}$ (kcal/mol)**	**Effect on affinity**
NP-A1N	147.5 ± 3.5	0.77	**
NP-N3A	66.2 ± 1.2	0.30	*
NP-E4A	37.6 ± 0.9	-0.03	*
NP-M6W	45.4 ± 1.5	0.07	*
NP-M6A	97.5 ± 2.2	0.53	*
NP-E7A	> 200	> 0.95	***
NP-T8A	> 200	> 0.95	***

NB: no binding observed at the highest concentration tested (200 μM). ΔΔG$_{eq}$ = RTln(Kd$_{mut}$/Kd$_{WT}$), where R is the gas constant and T is the temperature in Kelvin. Effect on affinity is negligible (*, less than 3-times the WT value), moderate (**, between 3 and 5-times the WT value) or critical (***, more than 5-times the WT value).

Table 2. NP1-B17 and NP2-B17 TCRs contacts with H-2D^b-NP$_{366}$

TCR gene	NP1-B17	NP2-B17	H-2D^b	Bond type
CDR3α-N	Glu108-Oε1	Glu108-Oε1-Oε2	Arg79-NH1	VDW, SB
CDR3α-N	Thr109		Gly16, Leu17, Glu18	VDW
CDR3α-N		Gly109	Glu18	VDW
CDR3α-J	Ser110		Leu82, Ala89	VDW
CDR3α-J		Ser110	Arg75, Arg79	VDW
CDR3α-J	Gly111	Gly111	Arg79	VDW
CDR3α-J	Ser112-Oγ		Glu18-Oε2, Arg75-NH2	VDW, HB
CDR3α-J		Ser112-Oγ	Glu18-Oε2	VDW, HB
CDR3α-J	Trp113	Trp113	Arg75, Val76, Arg79,	VDW
CDR3α-J	Gln114-Oε1	Gln114-Oε1	Arg79-NH2	VDW, HB
CDR2β	Tyr57	Tyr57	Gln72	VDW
CDR2β	Ile64	Ile64	Gly69, Trp73	VDW
FWβ	Asn66-Oδ1	Asn66-Oδ1	Val76, Asn80-Nδ2	VDW, HB
FWβ	Arg67-O-NH2	Arg67-O-NH2-NH1	Lys146-Nζ-0, Gln149-Oε1, Ser150	VDW, HB
FWβ	Phe72		Ile142, Arg145, Lys146, Gln149	VDW
FWβ		Phe72	Ile142, Arg145, Lys146	VDW
FWβ	Glu74	Glu74-N	Gln149-Oε1	VDW, HB
FWβ	Phe76		Gln149	VDW
FWβ	Gln77	Gln77	Gln149	VDW
CDR3β-D	Leu110-O	Leu110	Gln72, Arg75-NH2-NH1, Val76	VDW, HB
CDR3β-N		Asp111-Oδ1-Oδ2	Glu18-Oε1, Arg75-NH1, Glu19	VDW, HB. SB
TCR gene	NP1-B17	NP2-B17	NP$_{366}$	Bond type
CDR2β	Ile64		Asn5, Met6, Thr8	VDW
CDR2β		Ile64	Thr8	VDW
CDR2β	Leu65-O	Leu65-O	Glu7, Thr8-Oγ1-N	VDW, HB
FWβ	Asn66-Oδ1	Asn66-Oδ1	Thr8-Oγ1	VDW, HB
FWβ	Arg67-NH2-Nε	Arg67-NH2-Nε	Glu7-Oε1-Oε2	VDW, SB

Abbreviations are as follows: FW, Framework residue; HB, hydrogen bond cut off distance 3.5 Å; SB, salt bridge cut off distance 5 Å; N, non-germline encoded; D, diversity; J, joining; VDW, van der Waals cutoff distance at 4 Å.

Supplemental Table 1. H-2D^b-NP$_{366}$-specific TCRs used for in vitro and in vivo expression

TCR	TRAV	CDR1α	CDR2α	CDR3α	TRAJ	TRBV	CDR1β	CDR2β	CDR3β	TRBJ
NP1-B17	14-2	DSTFNY	IRSVSDK	CAASETSGSWQLIFG	22	17	MNHDT	YYDKIL	CASSRDLGRDTYQYFG	2-5
NP2-B17	14-2	DSTFNY	IRSVSDK	CAASEGSGSWQLIFG	22	17	MNHDT	YYDKIL	CASSAGLDAEQYFG	2-1
NP3-B17	12-2	STYSPF	SFTDNKR	CASNTGYQNFYFG	49	17	MNHDT	YYDKIL	CASSRGTGAGNTLYFG	1-3
NP1-B13	16	TRDSSYF	QDSYKKEN	CAMRVSGGSNAKLTFG	42	13-1	NSHNY	SYGAGN	CASSGGANTGQLYFG	2-2
NP2-B13	16	TRDSSYF	QDSYKKEN	CAMRANSGTYQRFG	13	13-1	NSHNY	SYGAGN	CASSGGANTGQLYFG	2-2
NP3-B13	16	TRDSSYF	QDSYKKEN	CAMRGSYGGRAQLIFG	15	13-1	NSHNY	SYGAGN	CASSGGANTGQLYFG	2-2
NP4-B13	16	TRDSSYF	QDSYKKEN	CAMREGLGQGGRALIFG	15	13-1	NSHNY	SYGAGN	CASSGGGNTGQLYFG	2-2
NP5-B13	16	TRDSSYF	QDSYKKEN	CAMRSAYQGGRALIFG	15	13-1	NSHNY	SYGAGN	CASSGGANTGQLYFG	2-2

Sequence in red denotes CDR3 region.

Supplemental Table 2. Data collection statistics

Data Collection Statistics	NP1-B17 TCR-H-2D^b-NP$_{366}$	NP2-B17 TCR-H-2D^b-NP$_{366}$
Temperature	100K	100K
Space group	$P\,2_12_12_1$	$P\,2_1$
Cell Dimensions (a,b,c) (Å)	92.23, 100.18, 469.46	48.02, 126.94, 80.48
(°)		$\beta = 105.66°$
Resolution (Å)	47.71 – 2.65	49.10 – 2.86
	(2.79 – 2.65)	(3.01 – 2.86)
Total number of observations	1850936 (272722)	90916 (13017)
Number of unique observations	127609 (18435)	21354 (3088)
Multiplicity	14.5 (14.8)	4.3 (4.2)
Data completeness (%)	100.0 (100.0)	99.0 (97.2)
I/σ_I	14.4 (2.0)	10.6 (2.3)
R_{pim}^{a} (%)	5.0 (59.1)	8.1 (38.3)
Refinement Statistics		
Non-hydrogen atoms		
Protein	26498	6617
Water	576	270
R_{factor}^{b} (%)	22.57	22.60
R_{free}^{b} (%)	24.88	27.23
Rms deviations from ideality		
Bond lengths (Å)	0.007	0.007
Bond angles (°)	0.95	0.87
Ramachandran plot (%)		
Favoured	91.4	93.7
Allowed	6.2	5.4
Disallowed	1.4	0.9

$^a R_{pim} = \Sigma_{hkl}\,[1/(N\text{-}1)]^{1/2}\,\Sigma_i\,|\,I_{hkl,\,i} - <I_{hkl}>\,|\,/\,\Sigma_{hkl}\,<I_{hkl}>$

$^b R_{factor} = \Sigma_{hkl}\,||\,F_o\,|\,\text{-}\,|\,F_c\,||\,/\,\Sigma_{hkl}|\,F_o\,|$ for all data except $\approx$ 5% which were used for R_{free} calculation.

Supplemental Table 3. Thermal stability of pMHC

H-2D^b-NP$_{366}$	Tm (°C)
WT	49.2 ± 0.7
Mutant H-2D^b with NP$_{366}$	**Tm (°C)**
E18A	47.6 ± 0.8
E19A	48.5 ± 0.5
Q65A	49.9 ± 0.5
K68A	50.3 ± 0.2
Q72A	56.9 ± 0.3
R75A	48.0 ± 0.5
V76A	51.0 ± 0.5
R79A	49.4 ± 0.2
N80A	49.6 ± 0.1
A89V	49.0 ± 0.5
K146A	41.8 ± 1.2
Q149A	45.4 ± 0.8
E163A	55.6 ± 0.2
H155A	48.1 ± 0.4
Q65A-G69A-H155A	47.8 + 0.8
H-2D^b with mutant NP$_{366}$	**Tm (°C)**
NP-A1N	43.7 ± 0.2
NP-N3A	47.0 ± 0.5
NP-E4A	51.8 + 0.1
NP-M6W	50.0 ± 0.5
NP-M6A	57.8 + 1.0
NP-E7A	49.3 + 0.2
NP-T8A	48.8 + 0.5

Supplemental Figure Legends

Supplemental Figure 1. Tetramer binding and functionality of H-2D^b-NP$_{366}$-specific TRBV17$^+$ and TRBV13-1$^+$ T cells after IAV infection.

(**a**) Levels of CD3ε staining on H-2D^b-NP$_{366}$-specific TRBV13$^+$ or TRBV17$^+$ CD8$^+$ T cells from spleens of mice at d10 after i.n. IAV infection. (**b**) Profiles of IFN-γ, TNF, and IL-2 staining following short term in vitro stimulation of NP1-B13 and NP1-B17 Rg cells harvested at d10 after co-transfer into recipient WT mice followed by IAV infection. (**c**) Proportion and (**d**) MFI of granzyme B production in NP1-B13 and NP1-B17 Rg cells at d7 after i.n. IAV infection.

Supplemental Figure 2. Reversed docking polarity of NP1-B17 compared with Treg and KIR binding.

Structure of the NP1-B17 TCR-H-2D^b-NP$_{366}$ complex (pink) superimposed on the structure of CD4 Treg-HLA-DR4-C19 (green) (**a**) and with KIR3DL1-HLA-B57-LSS (yellow) (**b**). The bottom panels are side view of the top panels.

Supplemental Figure 3. NP1-B17 TCR affinity measurement for H-2D^b-NP$_{366}$ and mutants.

Binding curves of the NP1-B17 TCR against a concentration range of H-2D^b-NP$_{366}$ complex and H-2D^b mutants (**a**) or NP$_{366}$ mutants (**b**) indicated by Response versus Concentration plots for duplicate experiments with error bars in black. Each H-2D^b-NP$_{366}$ complex is represented in colour, and the H-2D^b mutants (**a**) are divided into 3 panels for clarity.
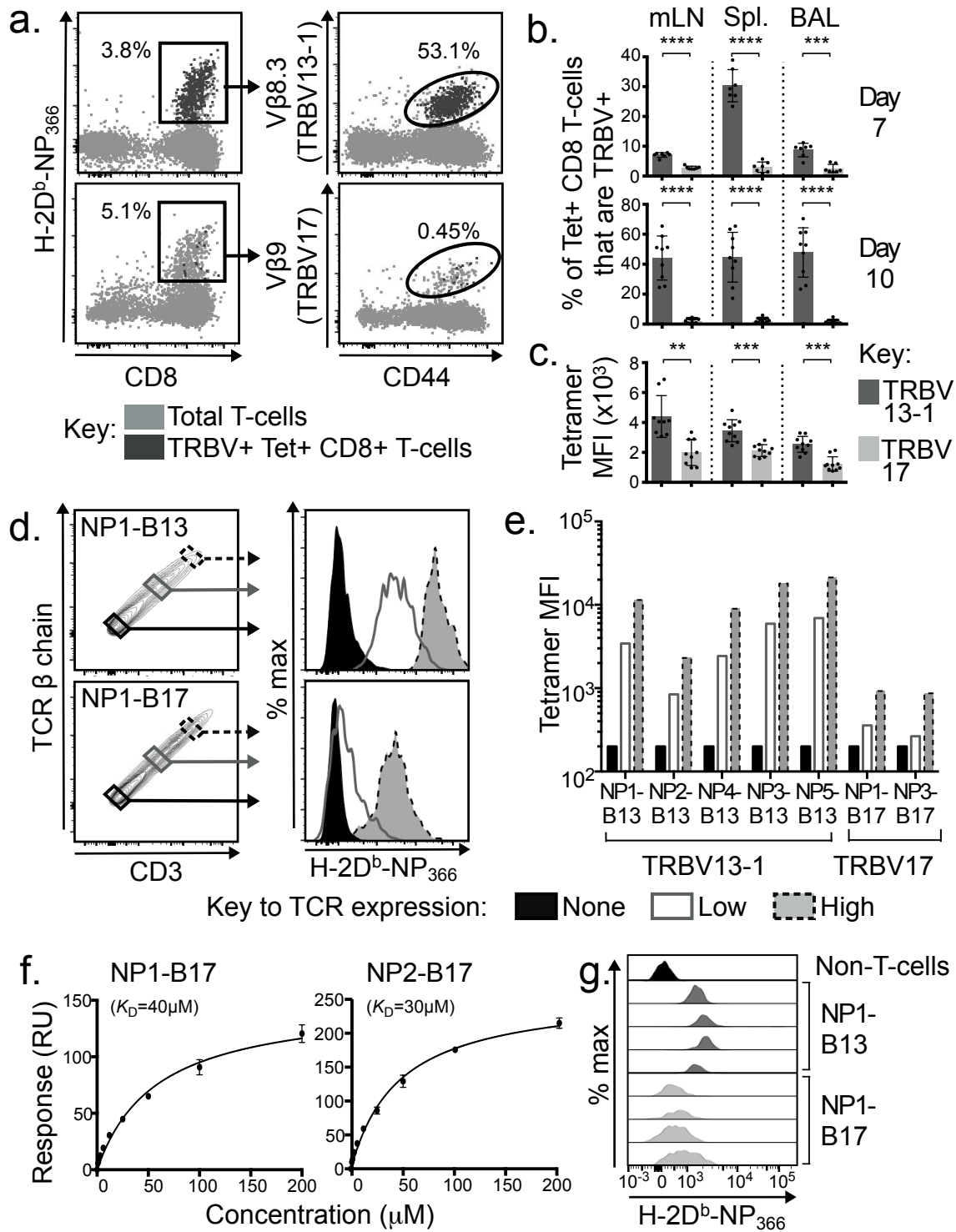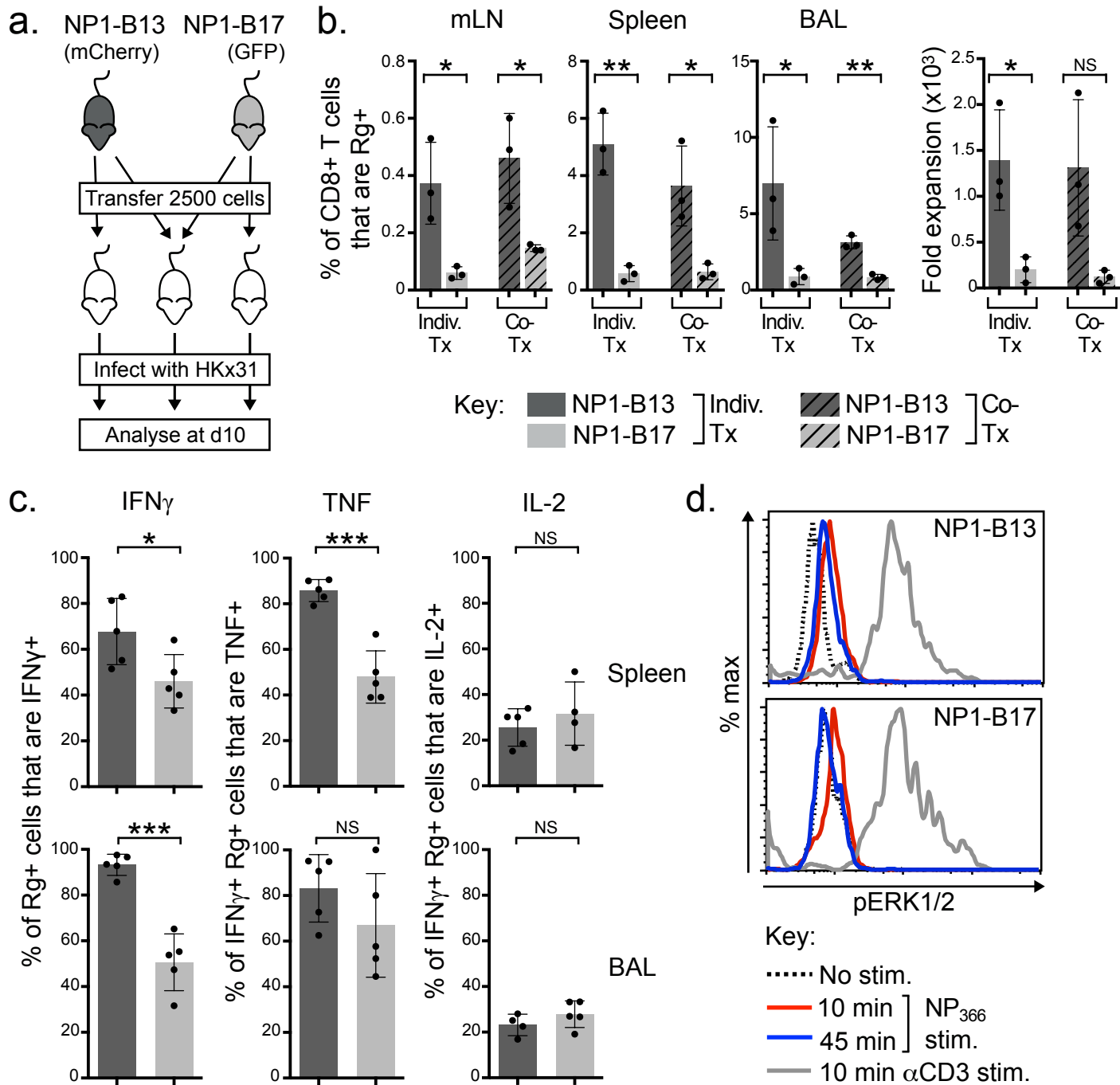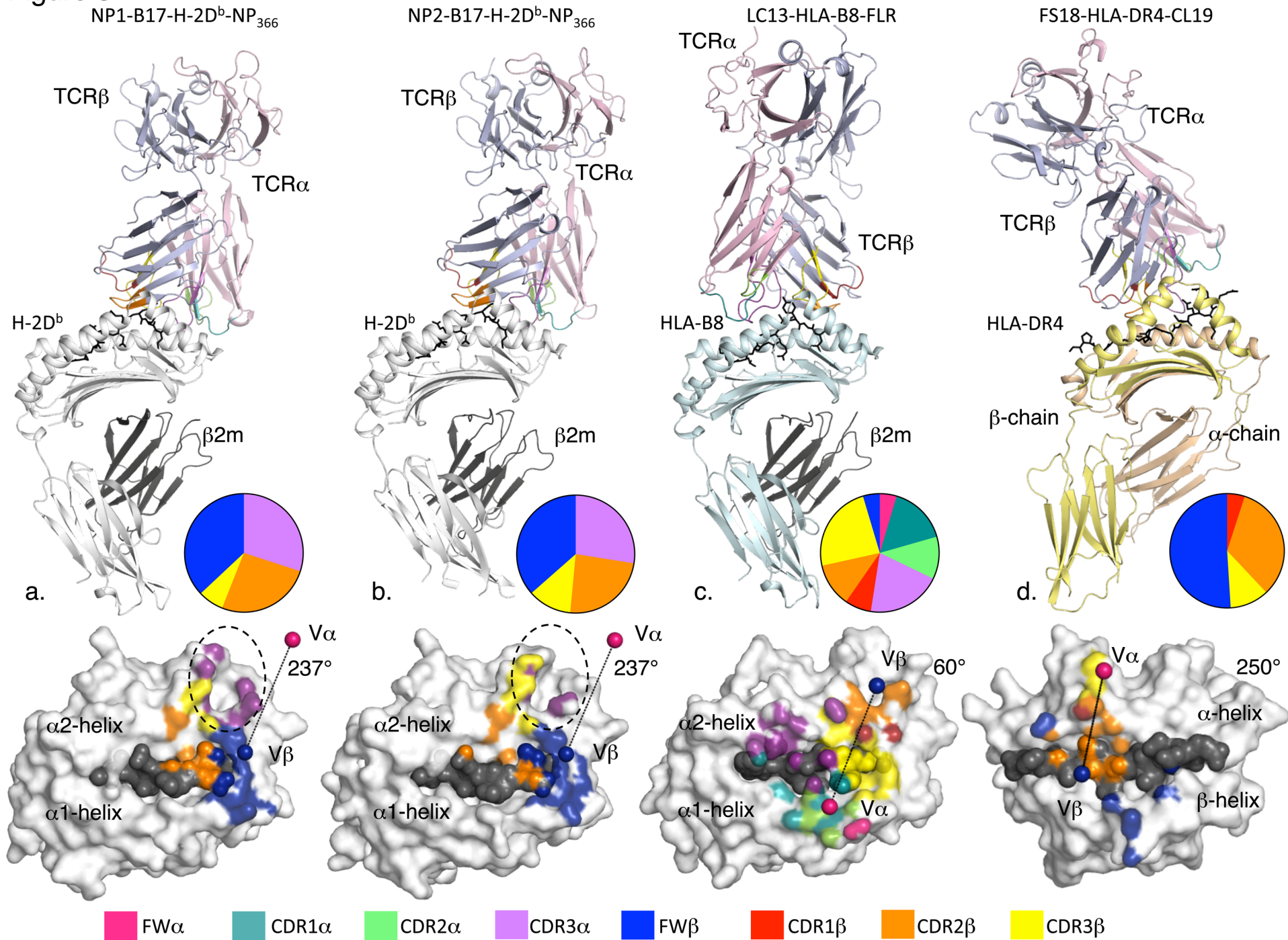
Figure1

Figure 1:

Figure2

Figure 2:

Figure 3

NP1-B17-H-2D^b-NP$_{366}$

NP2-B17-H-2D^b-NP$_{366}$

LC13-HLA-B8-FLR

FS18-HLA-DR4-CL19

a.

b.

c.

d.

TCRβ   TCRα   H-2D^b β2m   Vα   237°   Vβ   α2-helix   α1-helix

HLA-B8   HLA-DR4   β-chain   α-chain   60°   250°   α-helix   β-helix

| FWα | CDR1α | CDR2α | CDR3α | FWβ | CDR1β | CDR2β | CDR3β |

Figure 4

Figure5

Figure 5

Figure S1:

a.

b.

c.

d.

Key:
- ▨ NP1-B13 ⎤ Indiv. Tx
- ▨ NP1-B17 ⎦
- ▨ NP1-B13 ⎤ Co-Tx
- ▨ NP1-B17 ⎦

Figure S2:

a.

b.

Figure S3:

a.

H-2D^b-NP-WT
H-2D^b-K68A-NP
H-2D^b-E18A-NP
H-2D^b-V76A-NP
H-2D^b-K146A-NP
H-2D^b-N80A-NP

H-2D^b-E19A-NP
H-2D^b-E163A-NP
H-2D^b-Q65A-NP
H-2D^b-Q149A-NP
H-2D^b-A89V-NP
H-2D^b-R79A-NP

H-2D^b-Q72A-NP
H-2D^b-H155A-NP
H-2D^b-65-69-155-NP
H-2D^b-R75-NP

b.

H-2D^b-NP-E4A
H-2D^b-NP-M6W
H-2D^b-NP-N3A
H-2D^b-NP-M6A
H-2D^b-NP-N1A
H-2D^b-NP-T8A
H-2D^b-NP-E7A

Response (RU)

Concentration (µM)
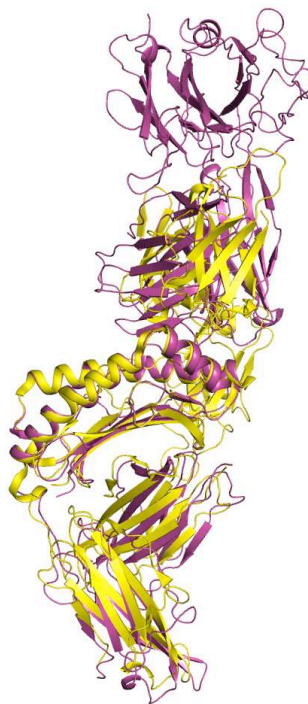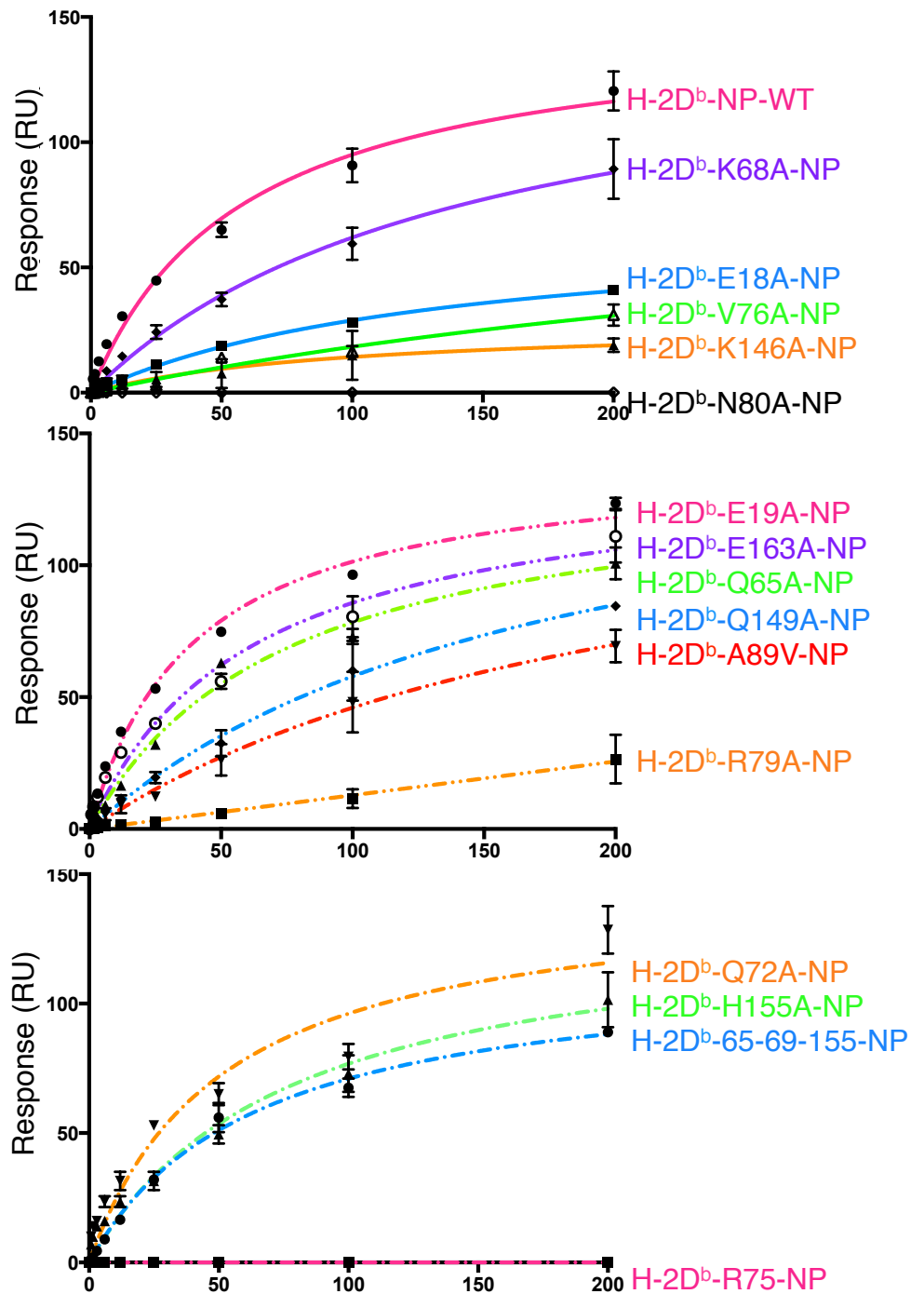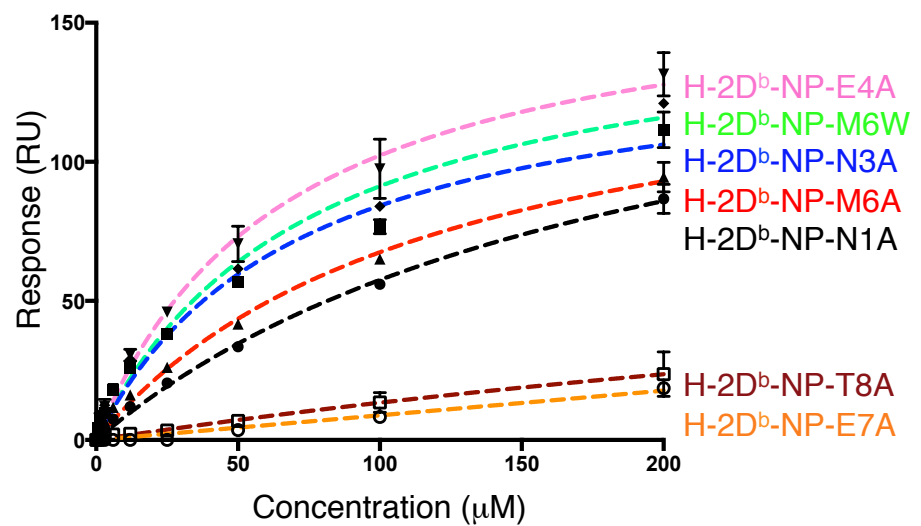
Supplemental Experimental Procedures

Generation of bone marrow-derived dendritic cells (BMDCs)

Bone marrow was obtained by flushing the tibia and femur of one 8 week old C57BL/6 mouse with D-PBS/2% FBS. Red blood cells were removed with Red Blood Lysing Solution™ (Sigma-Aldrich). Bone marrow cells ($6x10^6$) were cultured in a 6 well dish in complete T-cell medium supplemented with 10% FBS and GM-CSF (10 ng/ml) (Peprotech) for 5 d at which point BMDCs were harvested and processed for T-cell signaling.

T-cell signaling

BMDCs ($1x10^5$) or DC2.4 cells (6×10^5) (provided as a kind gift from Professor Kenneth Rock, University of Massachusetts Medical School) were incubated with or without 1 μM NP peptide for 1h at 37°C. Cells were re-suspended with $3x10^4$ FACS-purified GFP$^+$ murine retrogenic NP1-B17, NP1-B13 T-cells, or a panel of 2×10^5 Jurkat transductants expressing NP1-B17 wt and mutant TCRs and briefly spun down to allow for cell-cell conjugation for the indicated time points. To assess T cell signaling after CD3-crosslinking $3x10^4$ FACS purified GFP$^+$ murine retrogenic NP1-B17 or NP1-B13 T-cells were incubated with 2.5 μg/ml hamster anti-mouse CD3ε (145-2C11) for 15 min on ice. Cells were washed and stimulated with 20 μg/ml rabbit anti-hamster IgG (Sigma) for 10 minutes at 37°C. T cells were fixed in BD Cytofix^{TM} Fixation Buffer (BD Biosciences) for 20 min at 37°C and permeabilized in methanol/acetone (50:50) overnight at -20°C. T-cells and TCR transductants were washed and processed for intracellular staining using either phospho-p44/42 MAPK (Erk1/2) Thr202/Tyr204 rabbit mAb (Cell Signaling) for 1h at room temperature followed by the incubation with rabbit IgG (H+L), F(ab')2 fragment DyLight 649 (Jackson ImmunoResearch), or Pacific Blue-conjugated mouse anti-human ERK1/2 (pT202/pY204) (clone 20A) mAb. T-cells and TCR transductants were washed and data was collected using a CyAn ADP (Beckman Coulter) or a LSRII flow cytometer (BD Biosciences) and analysed using FlowJo8.7.7 (Tree Star Inc.) software. For cell sorting, an Influx (BD Biosciences) sorter was used.

Protein expression, purification, crystallisation and structure determination

The NP1-B17 and NP2-B17 TCRs as well as the wt and mutants pMHC complex were expressed, refolded and purified as previously described (Day et al., 2011).

Crystals of the NP1-B17 and NP2-B17 TCRs-H-2D^b-NP$_{366}$ complexes (5mg/ml) were grown by the vapour-diffusion method at 20°C in 10mM Tris-HCl pH 8, 150mM NaCl using 17% PEG 3350, 0.2 M K-Na-tartrate and 0.1 M Bis-Tris-Propane pH 7.5, and soaked in a cryoprotectant solution containing PEG concentration increased to 30%(w/v) and flash frozen in liquid nitrogen. The data was collected on the MX2 beamline at the Australian Synchrotron, Clayton using the ADSC-Quantum 315r CCD detector, processed using the XDS software (Leslie, 1992) and scaled using SCALA software (Evans, 2006) from the CCP4 suite (Winn et al., 2011). The structures were determined by molecular replacement using the PHASER (Read, 2001) program with the LC13 TCR as the search model for the TCR (Protein Data Bank accession number, 1KGC (Kjer-Nielsen et al., 2002)) and the H-2D^b for the MHC model without the peptide (Protein Data Bank accession number, 4HUU (Valkenburg et al., 2013)). Manual model building was conducted using the Coot software (Emsley and Cowtan, 2004) followed by maximum-likelihood refinement with the Buster program {Bricogne G., 2011 #276}. The TCRs were numbered according to the IMGT unique numbering system (Lefranc, 2003) whereby the CDR1 loops start at residue number 27, the CDR2 loops start at number 56, and the CDR3 loops start at residue number 105. The final model has been validated using the Protein Data Bank validation web site and the final refinement statistics are summarised in **Supplementary Table 2**.

All molecular graphics representations were created using PyMol (DeLano, 2002).

Thermal stability assay

To assess the effect of each mutation on the pMHC complex stability, a thermal shift assay was performed. The fluorescent dye Sypro orange was used to monitor the protein unfolding. The thermal stability assay was performed in the Real Time Detection system (Corbett RotorGene 3000), originally designed for PCR. Each pMHC complex was in 10 mM Tris-HCl pH8, 150 mM NaCl, at two concentrations (5 and 10 µM) in duplicate, was heated from 29 to 95°C with a heating rate of 1°C/min. The fluorescence intensity was measured with excitation at 530 nm and emission at 555 nm. The Tm, or thermal melt point, represents the temperature for which 50% of the protein is unfolded. Results are reported in **Supplementary Table 3**.

Surface Plasmon Resonance Measurement and Analysis

All surface plasmon resonance experiments were conducted at 25°C on the BIAcore 3000 instrument with 10mM Tris-HCl, pH 8, 150mM NaCl, 0.005% surfactant P20 and % BSA buffer. The NP1-B17 and NP2-B17 TCRs, as well as a negative control (LC13 (Gras et al., 2009)), bound to a CM5 sensor chip via amine coupling, and the pMHC was flown over the TCRs with a maximum concentration of 200 µM. The experiment was conducted as previously described (Gras et al., 2009) in duplicate with n=2. BIAevaluation Version 3.1 was used for data analysis with the 1:1 Langmuir binding model, the results are summarized in **Table 1**.